


 Cite this: *RSC Adv.*, 2021, **11**, 11793

DFT calculations bring insight to internal alkyne-to-vinylidene transformations at rhodium PNP- and PONOP-pincer complexes†

Nasir A. Rajabi * and Claire L. McMullin

Density Functional Theory (DFT) has been used to investigate the alkyne-to-vinylidene isomerisation reaction mediated by $[\text{Rh}(\text{PONOP})]^+$ complexes ($\text{X} = \text{CH}_2$: 2,6-bis(di-*tert*-butylphosphinomethyl)pyridine (PNP) and $\text{X} = \text{O}$: 2,6-bis(di-*tert*-butylphosphinito)pyridine (PONOP)) for terminal alkynes $\text{HC}\equiv\text{CR}$, where $\text{R} = {^t\text{Bu}}$ and $\text{Ar}' (3,5-{^t\text{Bu}_2\text{C}_6\text{H}_3})$. Calculations suggest the reaction mechanism proceeds *via* the slippage of π -bound alkyne at the Rh centre into a Rh–alkyne $\sigma_{\text{C}-\text{H}}$ complex followed by an indirect 1,2-H shift to give the Rh–vinylidene species. NBO (Natural Bond Orbital) analysis of the transition states corresponding to the latter indirect 1,2-H shift step indicates that the migrating hydrogen atom exhibits protic character and hence, the basicity of the H-accepting centre (C_β) is controlled by the substituents at that same atom and can tune the 1,2-H shift transition state. QTAIM (Quantum Theory of Atoms in Molecule) and NBO analyses of the Rh–vinylidene complexes indicate that these species exhibit a Rh \leftarrow C dative bond as well as π -back bonding from the Rh centre into the empty p_z orbital of the carbene centre (C_α), showing the Rh–vinylidene complexes are Fischer type carbenes. Analysis of the alkyne and vinylidene complex HOMOs show that the equilibrium between the isomers can be tuned by the P–Rh–P bite angle of the $[\text{Rh}(\text{pincer})]^+$ fragment. Dictated by the nature of the pincer backbone, wider bite angles shift the equilibrium toward the formation of the Rh–vinylidene isomer (e.g., $\text{X} = \text{CH}_2$ and $\text{R} = \text{Ar}'$), while tighter bite angles shift the equilibrium more to the formation of the Rh–alkyne isomer (e.g., $\text{X} = \text{O}$ and $\text{R} = \text{Ar}'$).

Received 14th October 2020

Accepted 3rd March 2021

DOI: 10.1039/d0ra08764e

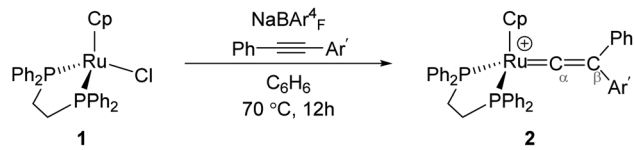
rsc.li/rsc-advances

Introduction

Transition metal (TM) vinylidene complexes are key species in organometallic chemistry.^{1–9} These compounds can be subjected to a variety of reactions such as hydrogenation, dehydrogenation and C–C bond formation processes.¹⁰ The most general strategy to form TM–vinylidene complexes under facile and simple conditions is the reaction of TM complexes with alkynes. This process can lead to the coordination of alkynes to a metal centre to give η^2 -alkyne complexes, which are stable enough to be characterised experimentally^{11–17} or can act as transient intermediates that undergo C–R ($\text{R} = \text{C}_6\text{H}_5$, Ar' and H) bond cleavage and migration of the R group to yield TM–vinylidene complexes.^{18–31} Such reactivity can be feasibly modulated by factors such as changing the nature of alkynes or the transition metal.

Mutoh, Ishii and co-workers described the reaction of $[\text{CpRu}(\text{dppe})]^+$ (**1**) (dppe = 1,2-diphenylphosphinoethane) with internal alkynes ($\text{PhC}\equiv\text{CAR}'$) and showed that both aryl

substituents undergo the 1,2-migration process to generate the disubstituted Ru–vinylidene species **2** (Fig. 1).^{16,32} They demonstrated that groups featuring electron-donating

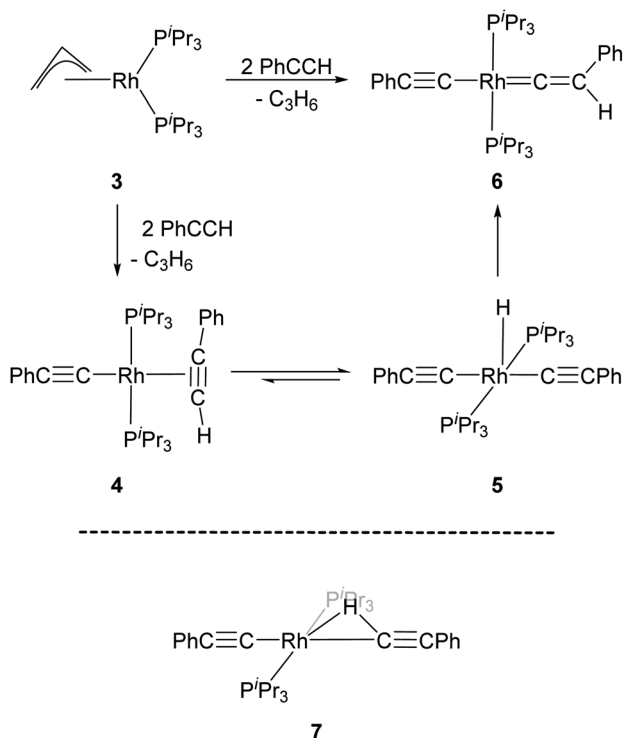


Ar'	Ar'-migration	Ph-migration
p-MeO-C ₆ H ₄	6%	94%
p-Me-C ₆ H ₄	23%	77%
p-Cl-C ₆ H ₄	55%	45%
p-CO ₂ Et-C ₆ H ₄	86%	14%

Fig. 1 Reaction of the Ru-precursor **1** with internal alkyne substrates $\text{PhC}\equiv\text{CAR}'$ to give the Ru–vinylidene species **2**.¹⁶

Department of Chemistry, University of Bath, Claverton Down, Bath, BA2 7AY, UK.
 E-mail: N.A.Rajabi@gmail.com

† Electronic supplementary information (ESI) available. See DOI: 10.1039/d0ra08764e



Scheme 1 Reaction scheme for the formation of the Rh-vinylidene species **6**,³⁴ and the DFT computed Rh–H alkenyl intermediate **7** featuring a bridging hydrogen between the Rh and C centres.³⁵

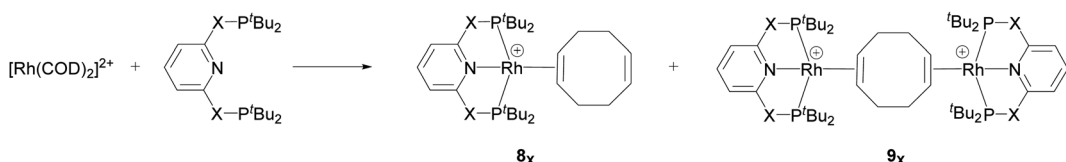
substituents decrease the relative migratory aptitude of the Ar' group over Ph. However, the migratory aptitude becomes opposite when Ar' groups have electron-withdrawing substituents. Based on these results, the authors suggested that this is due to the stabilisation of the negative charge on the Ar' group in the 1,2-Ar' shift transition state, suggesting the 1,2-Ar' migration proceeds *via* an electrophilic mechanism (Fig. 1).¹⁶ DFT (Density Functional Theory) studies by Tsuchida, Takano and co-workers on internal alkyne transformations at $[\text{CpRu}((\text{C}_6\text{H}_5)\text{C}\equiv\text{CC}_6\text{H}_4\text{R}-\text{p})(\text{dppe})]^+$ ($\text{R} = \text{OMe}, \text{CO}_2\text{Et}$) into the corresponding vinylidene complexes shows that this reaction proceeds with a direct 1,2-migration mechanism.³³ In accordance with the experimental findings of Ishii *et al.*, Tsuchida, Takano and co-workers showed that alkyne substrates with an electron-donating substituent ($\text{R} = \text{OMe}$) favours the Ph-migration over the Ar'-migration reaction. However, using NBO (Natural Bond Orbital) donor-acceptor interaction analysis, they stated that this reaction proceeds *via* a nucleophilic

mechanism; as in the 1,2-Ar'/Ph migration process, the electron-donating substituted Ar' group stabilises the positive charge of the accepting carbon centre (C_β), which facilitates the 1,2-Ph migration process.

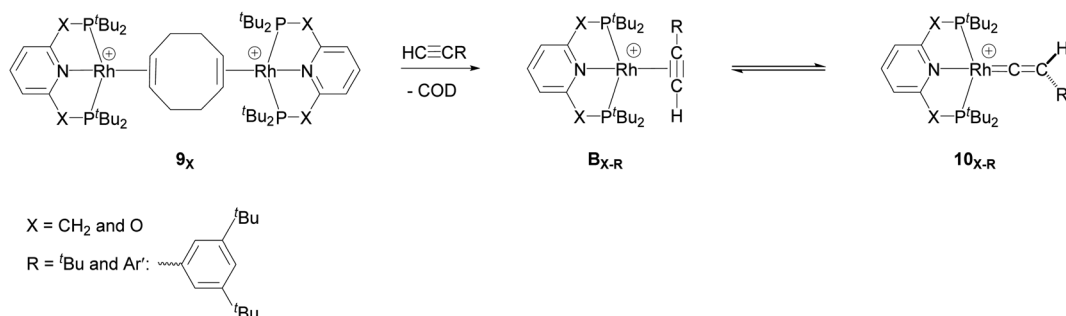
Werner and co-workers proposed the reaction of $[(\eta^3\text{-C}_3\text{H}_5)\text{Rh}(\text{P}^i\text{Pr}_3)_2]$ (3) with terminal alkynes $\text{HC}\equiv\text{CR}$ ($\text{R} = \text{H}, \text{Me}, \text{'Bu}$ and Ph) eliminates C_3H_6 and yields the Rh-alkyne species 4, which undergoes a C-H bond oxidative cleavage at the Rh centre to form the Rh-H species 5 (Scheme 1).³⁴ Complex 5 then undergoes a further transformation and gives the Rh-vinylidene species, 6. A DFT study by Hall and co-workers featured these reaction systems and shows that oxidative cleavage of the first $\text{HC}\equiv\text{CR}$ substrate ($\text{R} = \text{Ph}$) followed by a C-H reductive elimination at the Rh centre releases propene and forms a Rh-alkenyl intermediate.³⁵ Addition of a second $\text{HC}\equiv\text{CR}$ substrate to the Rh-alkenyl intermediate forms the bridging hydrogen intermediate 7 (Scheme 1), through which the H-migration proceeds with a 1,2-H shift mechanism to give $[(\text{PhC}\equiv\text{C})\text{Rh}(\text{P}^i\text{Pr}_3)_2(\text{C}=\text{C}(\text{Ph})(\text{H})]$ (6).

A DFT study by Angelis and co-workers on the isomerisation of $[(\text{Cp})(\text{PMe}_3)_2\text{Ru}(\text{HC}\equiv\text{CR})]^+$ to the vinylidene isomer shows that this reaction proceeds *via* an indirect 1,2-H shift reaction.³⁶ The second possible pathway to from the vinylidene isomer is the C–H oxidative cleavage of the alkyne at the Ru centre followed by a 1,3-H migration reaction to give the Ru–vinylidene complex. However, this was reported to be kinetically inaccessible, as the energy barrier of the 1,3-H shift reaction is significantly higher than the 1,2-H shift pathway. Later on, the same authors demonstrated that upon increasing the electron-richness of the Ru centre, the oxidative cleavage product can be both kinetically and thermodynamically accessible.³⁷ Particularly notable is the joint experimental and computational study by Lynam, Fey and co-workers on factors such as the nature of substituents, the metal and the ligands, which can control the thermodynamic preference of metal–vinylidene isomers over the corresponding metal–alkyne isomers.³⁸ The authors proposed a protocol to design ideal conditions to stabilise metal–vinylidene isomers. For instance in $[\text{RuCl}_2(\text{PR}'_3)(=\text{C}=\text{CHR})]$, with electron-withdrawing substituents (R) and phosphine ligands with electron-rich groups (R'), formation of the Ru–vinylidene isomer is thermodynamically favoured over the Ru–alkyne isomer.

Recently, Chaplin and co-workers described the substitution reaction in $[\text{Rh}(\text{COD})_2][\text{BAr}^F_4]$ with the pincer ligands $\text{P}(\text{X})\text{N}(\text{X})\text{P}(\text{X})$ ($\text{COD} = 1,5\text{-cyclooctadiene}$, $\text{Ar}^F = 3,5\text{-(CF}_3\text{)}_2\text{C}_6\text{H}_3$) ($\text{X} = \text{CH}_2$; $2,6\text{-bis}(\text{di-}tert\text{-butylphosphinomethyl})\text{pyridine}$ (PNP) and $\text{X} = \text{O}$; $2,6\text{-bis}(\text{di-}tert\text{-butylphosphinito})\text{pyridine}$ (PONOP)) which leads



Scheme 2 Reaction of the pincer ligand with the dimeric Rh precursor, $[\text{Rh}(\text{COD})_2]^{2+}$, to form 8_x and 9_x . The counter ions (BAr^{F}_4) are omitted for clarity.³⁹



Scheme 3 Reaction of the dimeric $\{\text{Rh}(\text{PNP})\}^{2+}$ complex **9_x** with terminal alkynes $\text{HC}\equiv\text{CR}$ ($\text{R} = {^t\text{Bu}}$ and $\text{Ar}' (3,5-{^t\text{Bu}_2}\text{C}_6\text{H}_3)$) to form the Rh-alkyne (**B_{x-R}**) and the Rh-vinylidene complex (**10_{x-R}**). The counter ions (BAr^{F_4}) are omitted for clarity.³⁹

to the formation of the corresponding PNP and PONOP-pincer complexes **8_x** and **9_x**.³⁹ As shown in Scheme 2, this reaction gives the monomeric complex **8_x** ($[\{\text{Rh}(\text{PNXNP})(\eta^2\text{-COD})\}[\text{BAr}^{\text{F}_4}]$) as the major product and the dimeric complex **9_x** ($[\{\text{Rh}(\text{PNXNP})\}_2(\mu\text{-}\eta^2\text{:}\eta^2\text{-COD})][\text{BAr}^{\text{F}_4}]$) as the minor product.

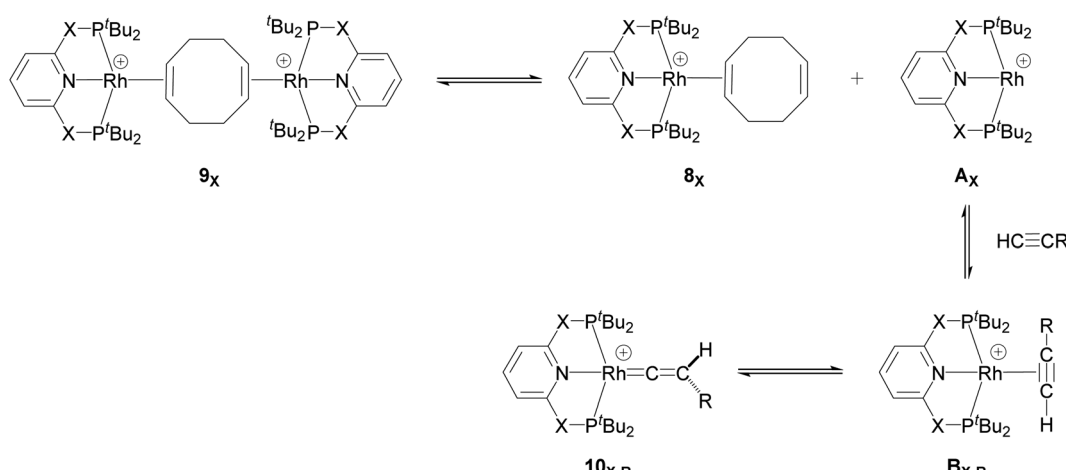
They demonstrated that reaction of the dimeric and monomeric Rh complexes **8_x** and **9_x** with L-type ligands such as CO results in the formation of the Rh-CO adduct, inferring the COD ligand dissociation from the Rh species forms the cationic $14\text{e}^- \{\text{Rh}(\text{pincer})\}^+$ species, which can be trapped out by CO to form the adduct. The authors also explored the reactivity of the active species, $\{\text{Rh}(\text{pincer})\}^+$, by the reaction of the dimeric complex **9_x** with $\text{HC}\equiv\text{CR}$ ($\text{R} = {^t\text{Bu}}$ and $\text{Ar}' (3,5-{^t\text{Bu}_2}\text{C}_6\text{H}_3)$) in 1,2-difluorobenzene (DFB) solvent at room temperature which gives the Rh-vinylidene complex **10_{x-R}** (Scheme 3).³⁹ With the dimeric $\{\text{Rh}(\text{PNP})\}^{2+}$, this process was found to be very fast (*ca.* five minutes) whereas, with the dimeric $\{\text{Rh}(\text{PONOP})\}^+$, it took significantly longer (*ca.* 18 h). It should be noted that with the dimeric $\{\text{Rh}(\text{PONOP})\}^{2+}$ and $\text{R} = \text{Ar}'$, this process forms the Rh-alkyne as the major product and the Rh-vinylidene complex as the minor product (70% *vs.* 30%). This suggests that the alkyne-to-vinylidene transformation process is reversible, a process

that is also seen at $[\text{RuCl}(\eta^5\text{-C}_9\text{H}_7)(\text{PPh}_3)_2]^{17}$ and $[\text{CpRu}(\text{dppe})]^+$ complexes.³²

Herein, DFT calculations were carried out to rationalise the mechanism of the formation of these Rh-vinylidene complexes, to characterise the nature of the Rh-carbene bond in the Rh-vinylidene complexes and to understand factors that can affect the equilibrium between the Rh-alkyne and Rh-vinylidene isomers.

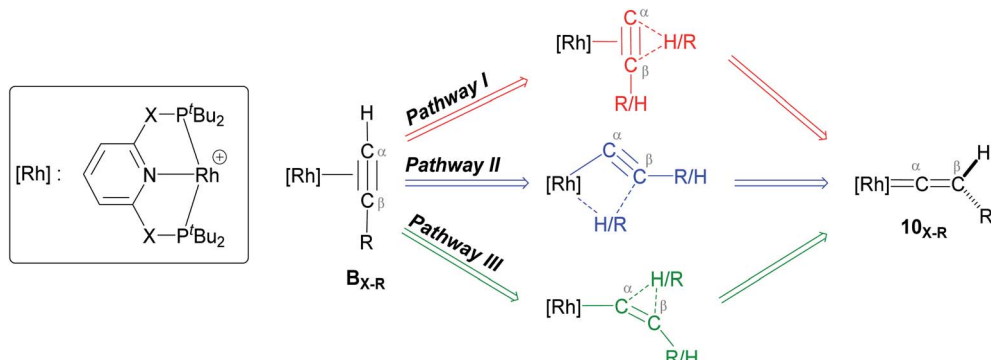
Computational methodology

Gas phase DFT calculations were run with Gaussian 09 (Revision D.01).⁴⁰ The Rh and P centres were described with the Stuttgart RECPs and associated basis sets,⁴¹ and the 6-31G** basis set was used for all other atoms (BS1).⁴² A polarization function was also added to P ($\zeta_d = 0.387$) and S ($\zeta_d = 0.503$) atoms. Initial BP86 (ref. 43 and 44) optimizations were performed using the 'grid = ultrafine' option, with all stationary points being fully characterized *via* analytical frequency calculations as either minima (all positive eigenvalues) or transition states (one negative eigenvalue). IRC (Intrinsic Reaction Coordinate) calculations and subsequent geometry optimizations were used to confirm the minima are linked by the isolated



Scheme 4 Formation of the 14e^- Rh species **A_x** and its onward reaction with the alkyne substrates to form the Rh-alkyne (**B_{x-R}**) and Rh-vinylidene species (**10_{x-R}**).



Scheme 5 Transition states for three potential mechanisms (Pathways I, II and III) to form the Rh-vinylidene complex 10_{X-R} .

transition state. All energies were recomputed with a larger basis set featuring cc-pVTZ-PP for Rh, cc-pVTZ-dk for S and the 6-311++G** basis set for all other atoms (BS2). 1,2-Difluorobenzene is not a parameter defined solvent in the Gaussian program. To overcome this its dielectric constant ($\epsilon = 13.4$) was specified when applying a polarizable continuum model solvent correction with BS1.⁴⁵ It should be noted that similar trends to the 1,2-difluorobenzene results were obtained when using fluorobenzene ($\epsilon = 5.42$, see ESI† for more details) as the solvation medium. Additional single-point dispersion corrections to the BP86 results employed Grimme's D3 parameter set with Becke-Johnson damping as implemented in Gaussian 09.⁴⁶ QTAIM (Quantum Theory of Atoms in Molecules)⁴⁷ and NBO (Natural Bonding Orbital)⁴⁸ were performed on the BP86-optimised geometries of the Rh-vinylidene complexes 10_{X-R} to characterise the nature of the Rh–carbene bond. The complete computational approach is described in shorthand as BP86-D3BJ (BS2,1,2-difluorobenzene)/BP86(BS1). All free energies are reported in kcal mol⁻¹ and are given relative to 9_X .

Results and discussion

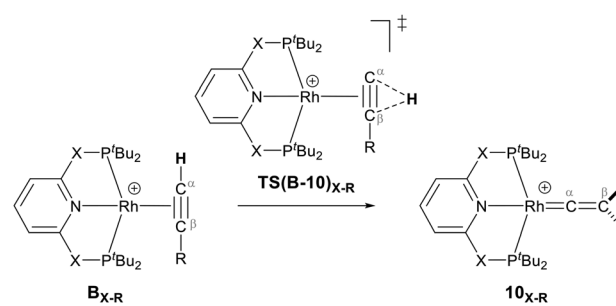
Our computed mechanism starts with the splitting of 9_X (as reported by Chaplin and co-workers³⁹) to give the $14e^-$ Rh species A_X (Scheme 4, X = CH₂ and O, R = ^tBu and Ar'). This process is endergonic by $\Delta G = +20.0$ kcal mol⁻¹ for X = CH₂ and $\Delta G = +23.0$ kcal mol⁻¹ for X = O. The cationic Rh moiety can be stabilised by the coordination of HC≡CR to A_X in a π -binding mode to the Rh centre to give the Rh–alkyne species B_{X-R} . For X = CH₂ and O and R = ^tBu, B_{X-tBu} lies at a free energy of -0.2 and -3.7 kcal mol⁻¹ respectively, showing formation of the PONOP complex (B_{O-tBu}) is energetically favoured by 3.5 kcal mol⁻¹. Coordination of HC≡Car' to the Rh centre significantly stabilises the cationic Rh species to form $B_{X-Ar'}$ at $\Delta G = -12.6$ kcal mol⁻¹ for X = CH₂ and $\Delta G = -11.0$ kcal mol⁻¹ for X = O.

As shown in Scheme 5, once the Rh–alkyne π -complex B_{X-R} has formed, it can undergo an intra-molecular transformation *via* three possible pathways (I, II and III) to afford the Rh–vinylidene complex 10_{X-R} . In Pathway I, the Rh–alkyne species B_{X-R} undergoes a direct 1,2-R/H migration to form 10_{X-R} . In Pathway II, transfer of the R/H groups onto the Rh centre occurs

via a four-member transition structure to yield 10_{X-R} . Pathway III proceeds with the initial formation of the Rh–C bond that induces the 1,2-H/R shift reaction simultaneously to give 10_{X-R} .

Both the ^tBu and Ar' alkyne substituents could migrate from the C_β centre to the C_α centre from B_{X-R} to form 10_{X-R} . However, the energy barriers for migration of Ar' or ^tBu groups *via* the pathways shown in Scheme 3 are computed to be too high (between 37 to 58 kcal mol⁻¹)⁴⁹ and hence, unsurmountable under the experimental reaction conditions of 9_X and HC≡CR³⁹ (see ESI, Tables S2 and S3†).

The most obvious route to form the Rh–vinylidene species involves H migration. In Pathway I (Table 1) for the PNP-pincer ligand and R = ^tBu, the direct 1,2-H shift reaction in B_{C-tBu} proceeds *via* $TS(B-10)_{C-tBu}$ at $\Delta G^\ddagger = +40.1$ kcal mol⁻¹ to afford the Rh–vinylidene species 10_{C-tBu} at $\Delta G = -12.1$ kcal mol⁻¹. The free energy barrier for this process ($\Delta\Delta G_1^\ddagger$) is computed to

Table 1 DFT calculated free energies^a (kcal mol⁻¹) for the transformation of the Rh–alkyne species B_{X-R} to the Rh–vinylidene species 10_{X-R} *via* Pathway I

X	R	B_{X-R}	$TS(B-10)_{X-R}$	$\Delta\Delta G_1^\ddagger$	10_{X-R}
CH ₂	^t Bu	-0.2	+40.1	40.3	-12.1
O	^t Bu	-3.7	+39.4	43.1	-8.9
CH ₂	Ar'	-12.6	+30.3	42.9	-15.7
O	Ar'	-11.0	+31.0	42.0	-10.9

^a DFT method = BP86-D3(BJ)-1,2-difluorobenzene/BS2//BP86/BS1. Computed energy barrier ($\Delta\Delta G_1^\ddagger$) is relative to B_{X-R} . All free energies are quoted relative to 9_X (X = CH₂ and O, R = ^tBu and Ar').

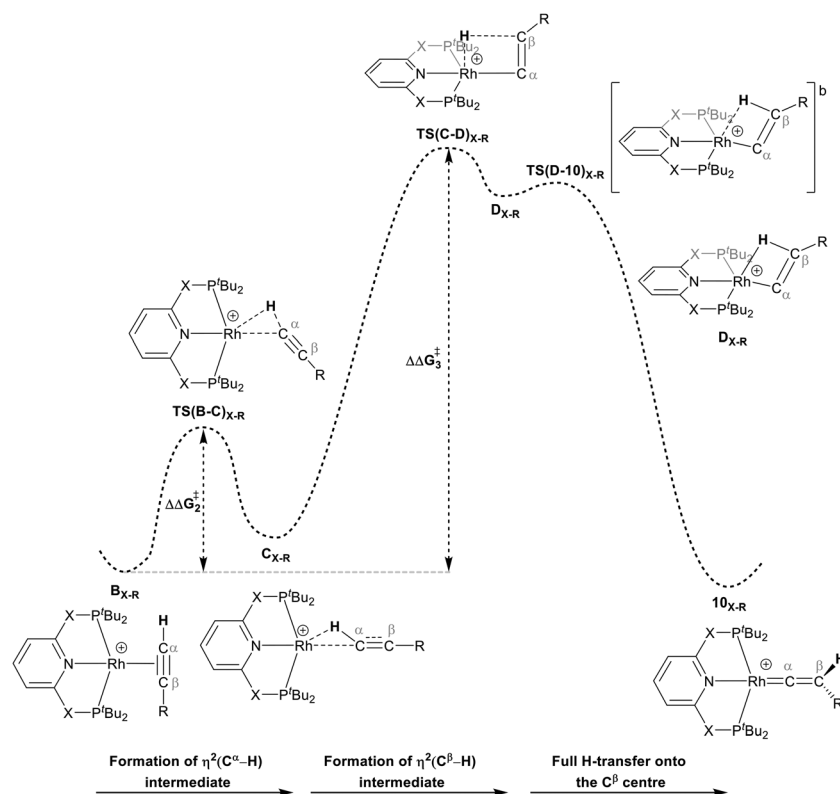


be 40.3 kcal mol⁻¹ (relative to $\mathbf{B}_{\text{C}-t\text{Bu}}$), which is too high to be accessible under the reaction conditions. Changing the pincer ligand from PNP to PONOP slightly lowers the free energy (by 0.7 kcal mol⁻¹) of the transition state corresponding to the 1,2-H shift process ($\mathbf{TS(B-10)_{O-t\text{Bu}}}$) to +39.4 kcal mol⁻¹ to give the Rh-vinylidene species $\mathbf{10}_{\text{O}-t\text{Bu}}$ at -8.9 kcal mol⁻¹. The free energy barrier for this process is still too high ($\Delta\Delta G_1^\ddagger = 43.1$ kcal mol⁻¹), going from $\text{R} = t\text{Bu}$ to $\text{R} = \text{Ar}'$, with the PNP-pincer ligand the transition state $\mathbf{TS(B-10)_{C-Ar}}$ lies at $\Delta G_1^\ddagger = +30.3$ kcal mol⁻¹; significantly lower than when $\text{R} = t\text{Bu}$. With respect to $\mathbf{B}_{\text{O-Ar}}$, the free energy barrier for this process is computed to be 42.9 kcal mol⁻¹ – again too high and not accessible at room temperature. A similar trend can be seen for the PONOP-pincer ligand when $\text{R} = \text{Ar}'$ ($\Delta\Delta G_1^\ddagger = 42.0$ kcal mol⁻¹). Therefore, the high energy barriers associated with the direct 1,2-H shift reaction in Pathway I are not in agreement with experiment.

For Pathway II (Table 2), $\mathbf{B}_{\text{C}-t\text{Bu}}$ undergoes slippage of the π -coordination mode to a $\sigma_{\text{C}-\text{H}}$ coordination mode *via* $\mathbf{TS(B-C)_{C-t\text{Bu}}}$ at $\Delta G_1^\ddagger = +8.8$ kcal mol⁻¹ to give $\mathbf{C}_{\text{C}-t\text{Bu}}$, featuring an elongated C_α -H bond (1.22 Å) to give a short $\text{Rh}\cdots\text{H}$ of 1.73 Å. NBO analysis of $\mathbf{C}_{\text{C}-t\text{Bu}}$ indicates a donor–acceptor interaction between the C_α -H bonding orbital and a vacant Rh orbital with stabilisation energy ($\Delta E^{(2)}$) of 82.9 kcal mol⁻¹, showing a C_α -H agostic interaction with the Rh centre (see ESI, Fig. S3† for details). With respect to $\mathbf{B}_{\text{C}-t\text{Bu}}$, formation of $\mathbf{C}_{\text{C}-t\text{Bu}}$ proceeds with a free energy barrier ($\Delta\Delta G_2^\ddagger$) of 9.0 kcal mol⁻¹ and is energetically downhill by 2.8 kcal mol⁻¹. $\mathbf{C}_{\text{C}-t\text{Bu}}$ can undergo the H-transfer into the bridging position between the C_β and Rh centre *via* $\mathbf{TS(C-D)_{C-t\text{Bu}}}$ at +37.7 kcal mol⁻¹ to give the four-membered intermediate $\mathbf{D}_{\text{C}-t\text{Bu}}$ at $\Delta G = +36.4$ kcal mol⁻¹.

The H atom then fully transfers onto the C_β centre to give $\mathbf{10}_{\text{C}-t\text{Bu}}$. Attempts to locate the transition state ($\mathbf{TS(D-10)_{X-R}}$) corresponding to this process were inconclusive as it was a very

Table 2 DFT calculated free energies^c (kcal mol⁻¹) for the transformation of the Rh–alkyne species $\mathbf{B}_{\text{X-R}}$ to the Rh–vinylidene species $\mathbf{10}_{\text{X-R}}$ *via* Pathway II

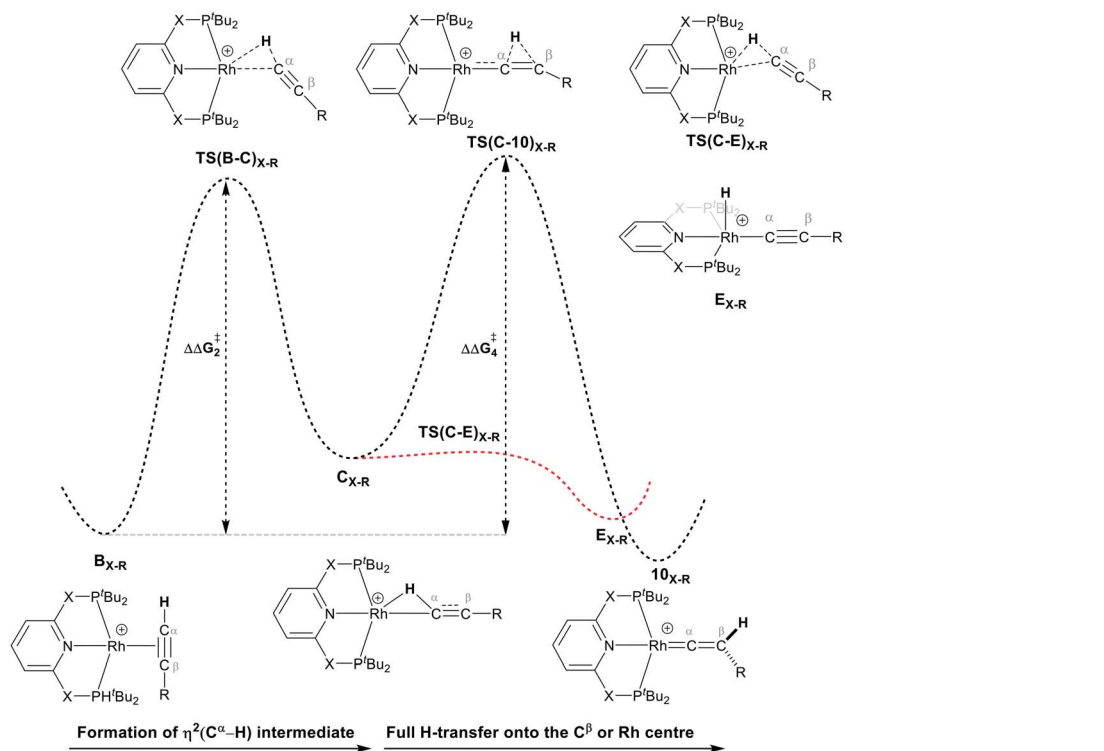


X	R	$\mathbf{TS(B-C)_{X-R}}$	ΔG_1^\ddagger	$\mathbf{C}_{\text{X-R}}$	$\mathbf{TS(C-D)_{X-R}}$	$\Delta\Delta G_2^\ddagger$	$\mathbf{D}_{\text{X-R}}$	$\mathbf{10}_{\text{X-R}}$
CH ₂	<i>t</i> Bu	+8.8	9.0	-3.0	+37.7	37.9	+36.4	-12.1
O	<i>t</i> Bu	+6.5	10.2	+1.3	+38.5	42.2	+37.0	-8.9
CH ₂	Ar'	+0.2	12.8	-4.5	+29.8 ^a	42.4 ^a	— ^b	-15.7
O	Ar'	+2.8	13.8	-1.0	+31.6 ^a	42.6 ^a	— ^b	-10.9

^a Estimated free energies by freezing the key distances in $\mathbf{TS(C-D)_{X-Ar'}}$. ^b Transition state is not calculated. ^c DFT method = BP86-D3(BJ)-1,2-difluorobenzene/BS2//BP86/BS1. Computed energy barriers ($\Delta\Delta G_2^\ddagger$ and $\Delta\Delta G_3^\ddagger$) are relative to $\mathbf{B}_{\text{X-R}}$. All free energies are quoted relative to $\mathbf{8}_X$ ($\text{X} = \text{CH}_2$ and O , $\text{R} = t\text{Bu}$ and Ar').



Table 3 DFT calculated free energies^a (kcal mol⁻¹) for the transformation of the Rh–alkyne species B_{X-R} to the Rh–vinylidene species 10_{X-R} (*via* Pathway III) and the Rh–H species E_{X-R}



X	R	TS(C-10) _{X-R}	C _{X-R}	ΔΔG ₄ [‡]	10 _{X-R}	TS(C-E) _{X-R}	E _{X-R}
CH ₂	^t Bu	+8.7	-3.0	8.9	-12.1	-2.8	-8.1
O	^t Bu	+10.2	+1.3	13.9	-8.9	+0.8	-0.6
CH ₂	Ar'	+7.6	-4.5	20.2	-15.7	-5.5	-11.4
O	Ar'	+9.1	-1.0	20.1	-10.9	-1.2	-4.4

^a DFT method = BP86-D3(BJ)-1,2-difluorobenzene/BS2//BP86/BS1. Computed energy barrier ($\Delta\Delta G_4^\ddagger$) is relative to B_{X-R} . All free energies are quoted relative to 9_X ($X = \text{CH}_2$ and O , $R = {^t\text{Bu}}$ and Ar').

flat potential free energy surface. A systematic increase of the Rh–H distance revealed that the energy barrier for this process is approximately 1.0 kcal mol⁻¹ (relative to $D_{C-t\text{Bu}}$). Thus, formation of $10_{C-t\text{Bu}}$ *via* Pathway II is a high energy-process that requires a free energy barrier ($\Delta\Delta G_3^\ddagger$) of 37.9 kcal mol⁻¹ (relative to $B_{C-t\text{Bu}}$). Likewise, for the PONOP ligand and $R = {^t\text{Bu}}$ formation of the $\sigma_{\text{C}-\text{H}}$ intermediate $C_{\text{O}-t\text{Bu}}$ ($C_\alpha-\text{H}$: 1.21 Å and $\text{Rh}\cdots\text{H}$: 1.75 Å, $\Delta E^{(2)} = 72.2$ kcal mol⁻¹) proceeds with a low free energy barrier ($\Delta\Delta G_2^\ddagger = 10.2$ kcal mol⁻¹). However, this process is energetically uphill by 5.0 kcal mol⁻¹, suggesting it can be reversed to reform the Rh–alkyne species $B_{\text{O}-t\text{Bu}}$. The H transfer into the bridging position between the Rh and C_β centres occurs *via* $TS(\text{C}-\text{D})_{\text{O}-t\text{Bu}}$ at $\Delta G^\ddagger = +38.5$ kcal mol⁻¹ to give $D_{\text{O}-t\text{Bu}}$ at $\Delta G = +37.0$ kcal mol⁻¹. A very flat free energy surface sees the full H-transfer onto the C_β centre to give $10_{\text{O}-t\text{Bu}}$ at $\Delta G = -8.9$ kcal mol⁻¹. Thus, for Pathway II, formation of the Rh–vinylidene species $10_{\text{O}-t\text{Bu}}$ requires a high free energy barrier of 42.2 kcal mol⁻¹. For $R = \text{Ar}'$ and the PNP-pincer ligand, the

transition state ($TS(\text{C}-\text{D})_{\text{C}-\text{Ar}}$) corresponding to the formation of the intermediate $C_{\text{C}-\text{Ar}}$ ($C_\alpha-\text{H}$: 1.19 Å and $\text{Rh}\cdots\text{H}$: 1.78 Å, $\Delta E^{(2)} = 73.9$ kcal mol⁻¹) has a free energy of 12.8 kcal mol⁻¹ – higher than when $R = {^t\text{Bu}}$ and computed to be energetically uphill by 8.1 kcal mol⁻¹. Unfortunately, all attempts to locate the four-member transition state ($TS(\text{C}-\text{D})_{\text{X}-\text{Ar}}$) corresponding to the H transfer onto the C_β centre and the subsequent intermediate $D_{\text{X}-\text{Ar}}$ remained allusive. Thus, the transition state free energy value was estimated by freezing the corresponding bond distances and $TS(\text{C}-\text{D})_{\text{C}-\text{Ar}}$ was calculated to be approximately $\Delta G^\ddagger = +29.8$ kcal mol⁻¹,⁵⁰ with a free energy barrier of 42.4 kcal mol⁻¹ that again is too high to be accessible under the reaction conditions. In comparison to the PNP ligand, the PONOP intermediate $C_{\text{O}-\text{Ar}}$ ($C_\alpha-\text{H}$: 1.18 Å and $\text{Rh}\cdots\text{H}$: 1.82 Å, $\Delta E^{(2)} = 67.1$ kcal mol⁻¹) formed *via* a slightly higher energy barrier ($\Delta\Delta G_2^\ddagger = 13.8$ kcal mol⁻¹). This process is computed to be more energetically uphill (by 1.9 kcal mol⁻¹). The H transfer process onto the C_β occurs with a high free energy barrier of



+42.6 kcal mol⁻¹ to form the Rh-vinylidene species. Thus, as outlined above, although formation of the σ_{C-H} intermediate C_{X-R} occur with low free energy barriers, the hydrogen transfer onto the C_β involves a large free energy barrier, which is not accessible under reaction conditions.

The indirect 1,2-H shift reaction *via* Pathway III involves the Rh sigma C–H complex C_{X-R} . As shown in Table 3, in C_{X-R} , the H centre can either transfer to the Rh centre to give E_{X-R} or it can transfer onto the C_β centre to form 10_{X-R} . The H-transfer onto the Rh centre occurs with a C–H oxidative cleavage at the Rh centre *via* $TS(C-E)_{X-R}$ to form the terminal Rh(III)–H species E_{X-R} . As listed in Table 3, in all cases, the H-transfer process to the Rh centre proceeds with a very flat free energy surface, an essentially barrierless process to give E_{X-R} , suggesting a facile reaction and importantly consistent with the findings reported by Hall and co-workers.³⁵ With respect to C_{X-R} , formation of the terminal Rh–H species E_{X-R} is slightly exergonic. However, E_{X-R} is considerably less thermodynamically favoured than the experimentally observed Rh-vinylidene species 10_{X-R} (by x kcal mol⁻¹).

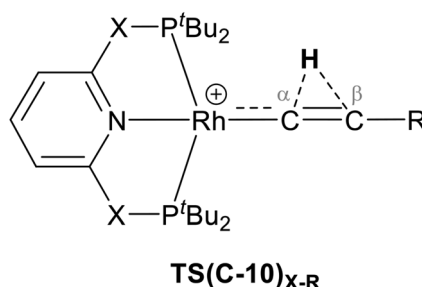
For the H transfer process onto the C_β centre *via* C_{X-R} , with $R = {^t}Bu$ and the PNP-pincer ligand, the bridging hydrogen indirectly can transfer onto the C_β centre *via* $TS(C-10)_{C-tBu}$, which lies at $\Delta G^\ddagger = +8.7$ kcal mol⁻¹ to generate 10_{C-tBu} . Interestingly, with respect to B_{C-tBu} , the free energy barrier for this process ($\Delta\Delta G_4^\ddagger$) is computed to be only 8.9 kcal mol⁻¹, significantly lower than those in Pathways I and II. With the PONOP-pincer ligand, the indirect 1,2-H shift process proceeds with a free energy barrier of 13.9 kcal mol⁻¹, which is 4.0 kcal mol⁻¹ higher than with the PNP-pincer ligand. The free energy barriers of the indirect 1,2-H migration process for the aryl-substituted alkyne with the PNP or the PONOP-pincer ligands increase to 20.2 kcal mol⁻¹ and 20.1 kcal mol⁻¹ respectively. However, they are significantly lower than those in Pathways I and II and values would be accessible at room temperature. Thus, Pathway III exhibits the energetically viable mechanism, consistent with the facile formation of Rh vinylidene species 10_{X-R} seen experimentally.

It should be noted that the Rh–H species E_{X-R} may undergo a reverse process *via* low free energy barriers (1.4–5.9 kcal mol⁻¹) to reform C_{X-R} and then follow the H-transfer reaction onto the C_β centre to generate 10_{X-R} which is more stable than the Rh–H species E_{X-R} . For $R = {^t}Bu$ and $X = CH_2$, the rate-determining step (RDS) is the indirect 1,2-H shift ($TS(C-10)_{X-R}$) while for other systems, RDS is the formation of the 14e⁻ Rh intermediate A_{X-tBu} .

Hydrogen character in the indirect 1,2-H shift reaction: protic or hydridic?

We have shown that formation of the Rh-vinylidene species proceeds *via* Pathway III, in which 1,2-H migration is a key step. However, it is not clear whether in the H-migration process, the H centre migrates as a proton or hydride (*i.e.*, *via* an electrophilic or a nucleophilic mechanism respectively). In this regard, as listed in Table 4, both $TS(C-10)_{C-tBu}$ and $TS(C-10)_{O-tBu}$ exhibit a shorter $C_\alpha \cdots H$ distance than $C_\beta \cdots H$ by 0.36 Å and 0.35 Å

Table 4 Key atomic distances (Å) and the NBO charges (a.u.) of selected atoms in the transition state $TS(C-10)_{X-R}$ – corresponding to indirect 1,2-H shift reaction



Structure	$C_\alpha \cdots H$	$C_\beta \cdots H$	Rh	H	C_α	C_β
$TS(C-10)_{C-tBu}$	1.18	1.54	-0.54	+0.39	-0.28	+0.06
$TS(C-10)_{O-tBu}$	1.18	1.55	-0.64	+0.39	-0.29	+0.09
$TS(C-10)_{C-Ar}$	1.22	1.41	-0.55	+0.40	-0.20	-0.04
$TS(C-10)_{O-Ar}$	1.24	1.36	-0.66	+0.40	-0.17	-0.06

respectively. This shows that the H centre exhibits a greater tendency to interact with the C_α centre than with the C_β centre. A similar trend can also be seen in $TS(C-10)_{C-Ar}$ and $TS(C-10)_{O-Ar}$ (0.19 Å and 0.12 Å respectively). However, for $R = Ar'$ the H centre has a considerably shorter distance to C_β , showing a stronger interaction between the H and C_β centres when $R = Ar'$. NBO charge analysis of the transition state $TS(C-10)_{X-R}$ shows that for $R = {^t}Bu$, the Rh centre exhibits a very similar negative charge value ($q_{Rh} = -0.54$ to -0.55), implying the nature of the X moiety in the pincer ligands has a negligible effect on the charge of the Rh centre. For $R = Ar'$, the Rh centre features a slightly more negative charge ($q_{Rh} = -0.64$ to -0.66) than when $R = {^t}Bu$, which can be attributed to the π -electrons of the aryl group of the alkyne. In all cases, the H centre features similar positive charges ($q_H = +0.39$ to $+0.40$), implying the H centre exhibits protic character, showing it can transfer *via* an electrophilic mechanism. For $R = {^t}Bu$, the C_β centre displays small positive charges, while for $R = Ar'$, the C_β centre possesses negative charges, indicating the electronic character of the C_β centre is sensitive to the nature of the R substituent. Interestingly, as the charge of the C_β centre becomes slightly negative (*e.g.*, $R = Ar'$), the transition state $TS(C-10)_{X-R}$ lies at a lower free energy (by 1.1 kcal mol⁻¹ for both PNP and PONOP relative to $R = {^t}Bu$), whereas, when the C_β has a positive charge (*e.g.*, $R = {^t}Bu$), the transition state $TS(C-10)_{X-R}$ lies at a higher free energy. This suggests that π -donor R substituents donate electron density to the empty C_β p_z orbital and hence increases its basicity, consistent with the electrophilic mechanism in the 1,2-H migration process. In order to examine this, the indirect 1,2-H shift process was computed for $X = CH_2$ and $R = NMe_2$. Our calculations show that the transition state $TS(C-10)_{C-NMe_2}$ exhibits a short $C_\beta \cdots H$ distance of 1.26 Å, showing a stronger interaction between the H and the C_β centres. This is due to NMe_2 being a strong π -donor substituent that significantly populates the C_β p_z orbital to give a more stable transition state



(at $\Delta G^\ddagger = +4.7$ kcal mol⁻¹), supporting the electrophilic character of the H centre in the indirect 1,2-H shift process.

Characterisation of the Rh-vinylidene complexes 10_{X-R} :

Fischer or Schrock-type complex?

TM-carbene complexes can be described as a Fischer or Schrock carbene complex, depending on the nature of the metal–carbene bond. In Fischer type carbene complexes, the carbene centre donates two electrons to the metal centre *via* a dative interaction whereas the metal centre donates electron density to the p_z orbital of the carbene centre through π -back bonding (*i.e.*, singlet carbene). In Schrock type carbene complexes, the carbene centre shares two single electron with the metal centre to form a σ and π metal–carbene bonds (*i.e.*, triplet carbene). Thus, the nature of the metal–carbene interactions in 10_{X-R} can provide useful information whether these species are Fischer or Schrock-type carbene complexes. In this context, in order to elucidate the nature of the metal–carbene bond in the Rh-vinylidene species 10_{X-R} , QTAIM and NBO analyses were performed on the BP86-optimised geometries of 10_{X-R} . As shown in Fig. 2, the QTAIM plot of 10_{C-tBu} exhibits a BCP (Bond Critical Point) along the Rh–C_α bond path, which is characterised by a positive Laplacian of electron density and small negative total energy density. This is indicative of a dative interaction between the Rh and carbene centres.⁵¹ A similar trend can also be observed for the other Rh-vinylidene species (see ESI, Fig. S4†). NBO analysis of 10_{C-tBu} identifies a Rh σ -bonding orbital that is dominated by carbene character (Rh (34.5%) and C_α (66.5%)), showing a Rh \leftarrow C_α dative interaction. Additionally, the NBO analysis reveals the presence of π -back donation from the Rh centre into the empty p_z orbital of the carbene, which is dominated by the Rh character (Rh (77.6%) and C_α (22.4%), see ESI, Fig. S4† for more details). Thus, the QTAIM and NBO data are fully consistent with a Rh(i) centre ligated by vinylidene (C_α=C_βHR) ligand and hence the Rh-vinylidene complexes 10_{X-R} can be described as a Fischer TM-carbene complex, seen previously in d⁸ TM-carbene complexes.⁵² It should be noted that in all the Rh-vinylidene complexes, the Rh–C_α σ -bond is polarised toward the C_α centre,

Table 5 The difference between the free energies of B_{X-Ar} and 10_{X-Ar} represented by ΔG_r (in kcal mol⁻¹) and HOMOs of B_{X-Ar} and 10_{X-Ar} and their difference represented by Δ_{HOMO} (in eV; X = NH, CH₂, O and S)

X	R	ΔG_r	HOMO (B_{X-R})	HOMO (10_{X-R})	Δ_{HOMO}
CH ₂	^t Bu	-11.9	-7.05	-7.31	+0.26
O	^t Bu	-5.2	-7.54	-7.65	+0.11
S	Ar'	-3.2	-7.25	-7.31	-0.06
CH ₂	Ar'	-3.1	-6.87	-6.96	-0.09
NH	Ar'	-2.1	-7.01	-7.04	-0.03
O	Ar'	+0.1	-7.29	-7.23	+0.06

while the Rh–C_α π -interaction is polarised toward the Rh centre (see ESI, Fig. S4†).

Stability of Rh-alkyne vs. Rh-vinylidene complexes

As shown above, for R = Ar' and the PNP pincer ligand, the Rh-vinylidene isomer is more stable than the Rh-alkyne isomer, while with the PONOP pincer ligand, the Rh-alkyne isomer is more stable. In order to explore the equilibrium between the Rh-alkyne and Rh-vinylidene isomers, the difference between the free energies of B_{X-R} and 10_{X-R} species were calculated and is represented by ΔG_r ($(\Delta G_r = \Delta G(10_{X-R}) - \Delta G(B_{X-R})$, Table 5). A negative ΔG_r value indicates that the equilibrium is toward the Rh-vinylidene isomer while a positive value indicates the equilibrium is toward the Rh-alkyne isomer. As listed in Table 5, our computational findings show that for R = ^tBu and both PNP or PONOP-pincer ligands, ΔG_r is negative, with the PNP-pincer complex being significantly more negative than the PONOP-pincer complex (-11.9 and -5.2 kcal mol⁻¹, respectively). For R = Ar' and the PNP-pincer ligand, ΔG_r is also negative (-3.1 kcal mol⁻¹) yet for the PONOP-pincer ligand ΔG_r becomes slightly positive (+0.1 kcal mol⁻¹). This trend implies that with the aryl substituent, the Rh-vinylidene complex is less stable than the alkyl substituent. This becomes critically important when switching from the PNP pincer ligand to the PONOP pincer ligand, as in this case, the Rh-alkyne isomer becomes more stable than the Rh-vinylidene isomer. This

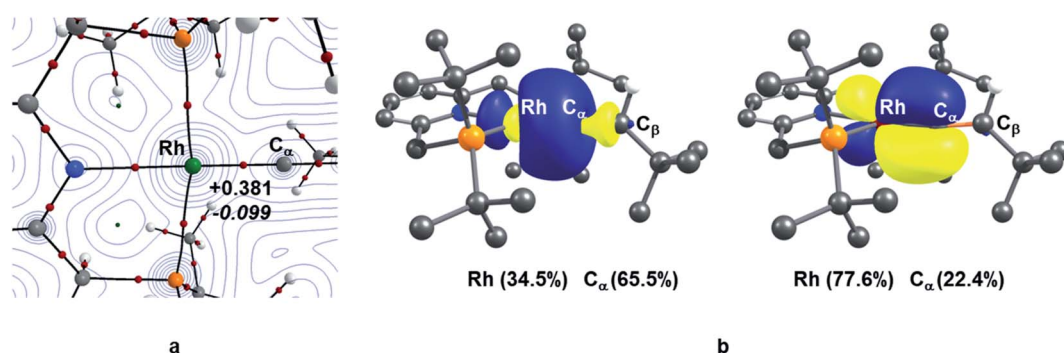


Fig. 2 (a) QTAIM molecular graph of 10_{C-tBu} ; the electron density contours are computed in the {Rh/P/C_α} plane with bond critical points (BCPs) shown as small red spheres; for the Rh–C_α BCP, the Laplacian of the electron density ($\nabla^2\rho(r)$ in eÅ⁻⁵, in plain) and total energy density ($H(r)$ in a.u., in italic) (b) NBO σ - and π -bonding orbitals of the Rh–C_α interaction and the contribution of the Rh and C_α centres in the corresponding interactions in 10_{C-tBu} .



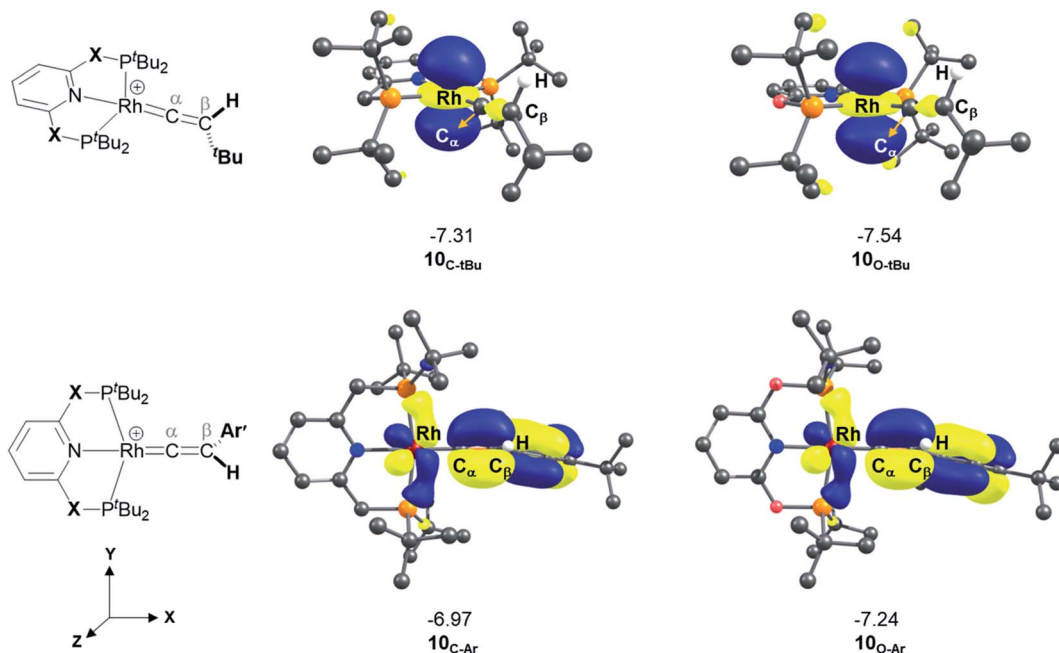


Fig. 3 HOMOs (in eV) of Rh–vinylidene species 10_{X-R} ($X = \text{CH}_2$ and O ; $R = {^t\text{Bu}}$ and Ar'). Substituent hydrogen atoms removed for clarity.

highlights the influence of the nature of both substituent and pincer ligand on the stability of the Rh–vinylidene species.

A detailed analysis of the electronic structure of the Rh–alkyne and Rh–vinylidene complexes can help to understand the origin of the equilibrium between the two isomers. As shown in Fig. 3, the molecular orbital analysis of the Rh–vinylidene species 10_{X-R} shows that when $R = {^t\text{Bu}}$, the HOMO of 10_{X-R} predominantly consists of the Rh d_{z^2} character, whereas for $R = \text{Ar}'$, the HOMO consists of the Rh d_{xy} orbital and the π -system of the aryl moiety. With the PNP-pincer ligand, when $R = \text{Ar}'$, the Rh–vinylidene complex exhibits a higher HOMO than when $R = {^t\text{Bu}}$ (-7.31 eV and -6.96 eV, respectively). This can be attributed to the presence of the π -system of the aryl moiety, which in conjugation with the $\text{C}_\alpha\text{–C}_\beta$ π -bond and the $\{\text{Rh}(\text{pincer})\}^+$ moiety can destabilise the HOMO of the system and hence affects the stability of the Rh–vinylidene complex. Thus, it suggests that the HOMO energy is a reasonable descriptor that can capture the stability of the Rh–vinylidene isomer *versus* the Rh–alkyne isomer.

Table 5 lists the energy difference between the HOMOs of \mathbf{B}_{X-R} and 10_{X-R} species, represented by Δ_{HOMO} ($\Delta_{\text{HOMO}} = \text{HOMO}(10_{X-R}) - \text{HOMO}(\mathbf{B}_{X-R})$). For $R = {^t\text{Bu}}$ and the PNP pincer ligand, Δ_{HOMO} is $+0.26$ eV, showing the Rh–vinylidene isomer possess a more stable HOMO than the Rh–alkyne isomer. Similarly, for $R = {^t\text{Bu}}$ and the PONOP pincer ligand, Δ_{HOMO} is also a positive value ($+0.11$ eV). However, the PONOP analogue has a smaller Δ_{HOMO} than the PNP complex. A similar trend can also be seen for $R = \text{Ar}'$ ($+0.09$ eV). Interestingly, for $R = \text{Ar}'$, when the pincer ligand is PONOP, the Rh–alkyne complex features a more stable HOMO than the Rh–vinylidene isomer ($\Delta_{\text{HOMO}} = -0.06$ eV). This suggests that for $R = \text{Ar}'$, the nature of the pincer ligand plays an important role on the stability of the

HOMO of the Rh–vinylidene isomer *versus* the Rh–alkyne isomer. In order to investigate this further, the relative free energies of the vinylidene complex against the alkyne isomer was also computed for $X = \text{NH}$ and S , and $R = \text{Ar}'$. Both $X = \text{NH}$ and S showed a similar trend to $X = \text{CH}_2$, with the Rh–vinylidene complex being more stable than the Rh–alkyne complex ($\Delta G_r = -2.1$ and -3.2 kcal mol $^{-1}$ respectively) in which the Rh–vinylidene isomer features a more stable HOMO than the Rh–alkyne isomer ($\Delta_{\text{HOMO}} = -0.03$ and -0.06 eV respectively). Interestingly, a reasonable correlation ($R^2 = 0.95$, Fig. S1 \dagger) was found between ΔG_r and Δ_{HOMO} values, showing when Δ_{HOMO} is negative, the Rh–vinylidene species is more stable than the Rh–alkyne species and when Δ_{HOMO} is positive, the Rh–alkyne species is more stable than the Rh–vinylidene species. This therefore indicates that for $R = \text{Ar}'$, Δ_{HOMO} can capture the stability of the Rh–vinylidene *versus* the Rh–alkyne species, however, raises the question; why is Δ_{HOMO} negative for $X = \text{CH}_2$, NH or S , while for $X = \text{O}$, Δ_{HOMO} is positive?

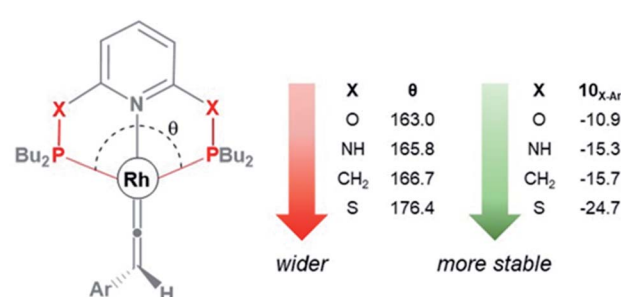


Fig. 4 The P–Rh–P bite angle (θ , in degree) and the free energy (kcal mol $^{-1}$) of the Rh–vinylidene species $10_{X-\text{Ar}}$.



As shown in Fig. 3, the HOMO of the Rh–vinylidene complex **10_{X-Ar}** consists of the Rh d_{xy} orbital that is affected by the P–Rh–P bite angle (θ) of the supporting pincer ligand. For X = O, the θ value of **10_{O-Ar}** is 163.0° and its HOMO energy is −7.23 eV (Fig. 4). In comparison to X = O, for X = S, the θ value of **10_{S-Ar}** is considerably larger (176.4°) and its HOMO is more stable than **10_{O-Ar}** (−7.31 eV). Interestingly, an excellent correlation ($R^2 = 0.9999$, Fig. S2†) was found between the free energy of the Rh–vinylidene species **10_{X-R}** and its θ value, showing tighter P–Rh–P bite angles result in more reactive Rh–vinylidene species (*i.e.*, higher HOMOs), while wider bite angles give more stable Rh–vinylidene species **10_{X-R}** (*i.e.*, lower HOMO), consistent with recent work from Mansell.⁵³ Thus, the bite angle is dictated by the nature of the X moiety and can therefore tune the reactivity of the Rh–vinylidene species *versus* the Rh–alkyne species **B_{X-R}**.

Conclusions

DFT calculations on the transformation of Rh–alkyne **B_{X-R}** into the Rh–vinylidene complex **10_{X-R}** reveal that this process involves the slippage of the Rh–alkyne π -complex into the Rh–alkyne σ_{C-H} complex – followed by an indirect 1,2-H shift reaction. The H atom in the indirect 1,2-H shift transition state has protic character. The presence of π -donor groups at the accepting carbon centre (C_B) can populate the C_B empty p_z orbital and hence increase its basicity to give stronger C_B···H interactions, which consequently lower the free energy of the 1,2-H shift transition state. The equilibrium between the alkyne and vinylidene species can be tuned by the P–Rh–P bite angle, which is dictated by the nature of the X moiety in the PNXNP pincer ligand coordinated to the Rh-centre.

Conflicts of interest

There are no conflicts to declare.

Acknowledgements

The authors acknowledge EPSRC (UK) for financial support under award EP/R020752/1 (CLM and NAR). This research made use of the Balena High Performance Computing (HPC) Service at the University of Bath. The authors would like to thank Adrian Chaplin (University of Warwick) for discussions on his group's experimental research that initiated this study.

Notes and references

- 1 F. Ye, J. Chen and T. Ritter, *J. Am. Chem. Soc.*, 2017, **139**, 7184–7187.
- 2 Y. Yamamoto, K. Matsui and M. Shibuya, *Chem.–Eur. J.*, 2015, **21**, 7245–7255.
- 3 S. Takano, T. Kochi and F. Kakiuchi, *Organometallics*, 2016, **35**, 4112–4125.
- 4 S. W. Roh, K. Choi and C. Lee, *Chem. Rev.*, 2019, **119**, 4293–4356.
- 5 L. Nunes dos Santos Comprido, J. E. M. N. Klein, G. Knizia, J. Kästner and A. S. K. Hashmi, *Chem.–Eur. J.*, 2016, **22**, 2892–2895.
- 6 F. Kakiuchi, S. Takano and T. Kochi, *ACS Catal.*, 2018, **8**, 6127–6137.
- 7 R.-S. Liu, *Synlett*, 2008, **2008**, 801–812.
- 8 B. M. Trost and J. T. Masters, *Chem. Soc. Rev.*, 2016, **45**, 2212–2238.
- 9 M. Otsuka, N. Tsuchida, Y. Ikeda, N. Lambert, R. Nakamura, Y. Mutoh, Y. Ishii and K. Takano, *Organometallics*, 2015, **34**, 3934–3943.
- 10 A. B. Antonova, *Coord. Chem. Rev.*, 2007, **251**, 1521–1560.
- 11 P. Barrio, M. A. Esteruelas and E. Oñate, *Organometallics*, 2003, **22**, 2472–2485.
- 12 M. J. Cowley, J. M. Lynam and J. M. Slattery, *Dalton Trans.*, 2008, 4552–4554, DOI: 10.1039/B806358C.
- 13 V. K. Singh, E. Bustelo, I. de los Ríos, I. Macías-Arce, M. C. Puerta, P. Valerga, M. A. Ortúñoz, G. Ujaque and A. Lledós, *Organometallics*, 2011, **30**, 4014–4031.
- 14 M. Jiménez-Tenorio, M. C. Puerta, P. Valerga, M. A. Ortúñoz, G. Ujaque and A. Lledós, *Inorg. Chem.*, 2013, **52**, 8919–8932.
- 15 Y. Ikeda, Y. Mutoh, K. Imai, N. Tsuchida, K. Takano and Y. Ishii, *Organometallics*, 2013, **32**, 4353–4358.
- 16 Y. Mutoh, Y. Ikeda, Y. Kimura and Y. Ishii, *Chem. Lett.*, 2009, **38**, 534–535.
- 17 M. Bassetti, V. Cadierno, J. Gimeno and C. Pasquini, *Organometallics*, 2008, **27**, 5009–5016.
- 18 D. B. Grotjahn, X. Zeng and A. L. Cooksy, *J. Am. Chem. Soc.*, 2006, **128**, 2798–2799.
- 19 W. Debrouwer and A. Fürstner, *Chem.–Eur. J.*, 2017, **23**, 4271–4275.
- 20 I. de los Ríos, E. Bustelo, M. C. Puerta and P. Valerga, *Organometallics*, 2010, **29**, 1740–1749.
- 21 P.-Y. Chia, C.-C. Kuo, S.-L. Huang, Y.-H. Liu, L.-K. Liu and Y.-C. Lin, *Chem.–Asian J.*, 2018, **13**, 3885–3894.
- 22 J. M. Lynam, C. E. Welby and A. C. Whitwood, *Organometallics*, 2009, **28**, 1320–1328.
- 23 R. H. Lam, D. B. Walker, M. H. Tucker, M. R. D. Gatus, M. Bhadbhade and B. A. Messerle, *Organometallics*, 2015, **34**, 4312–4317.
- 24 F. Mo, H. N. Lim and G. Dong, *J. Am. Chem. Soc.*, 2015, **137**, 15518–15527.
- 25 V. Cadierno, M. P. Gamasa, J. Gimeno, C. González-Bernardo, E. Pérez-Carreño and S. García-Granda, *Organometallics*, 2001, **20**, 5177–5188.
- 26 M. Bassetti, P. Alvarez, J. Gimeno and E. Lastra, *Organometallics*, 2004, **23**, 5127–5134.
- 27 I. Jourdain, L. Vieille-Petit, S. Clément, M. Knorr, F. Villafañe and C. Strohmann, *Inorg. Chem. Commun.*, 2006, **9**, 127–131.
- 28 M. J. Cowley, J. M. Lynam and A. C. Whitwood, *J. Organomet. Chem.*, 2010, **695**, 18–25.
- 29 J. M. Lynam, *Chem.–Eur. J.*, 2010, **16**, 8238–8247.
- 30 D. G. Johnson, J. M. Lynam, J. M. Slattery and C. E. Welby, *Dalton Trans.*, 2010, **39**, 10432–10441.
- 31 F. De Angelis, A. Sgamellotti and N. Re, *Organometallics*, 2007, **26**, 5285–5288.



32 Y. Mutoh, K. Imai, Y. Kimura, Y. Ikeda and Y. Ishii, *Organometallics*, 2011, **30**, 204–207.

33 M. Otsuka, N. Tsuchida, Y. Ikeda, Y. Kimura, Y. Mutoh, Y. Ishii and K. Takano, *J. Am. Chem. Soc.*, 2012, **134**, 17746–17756.

34 M. Schäfer, J. Wolf and H. Werner, *Organometallics*, 2004, **23**, 5713–5728.

35 B. A. Vastine and M. B. Hall, *Organometallics*, 2008, **27**, 4325–4333.

36 F. De Angelis, A. Sgamellotti and N. Re, *Organometallics*, 2002, **21**, 5944–5950.

37 F. De Angelis, A. Sgamellotti and N. Re, *Dalton Trans.*, 2004, 3225, DOI: 10.1039/b408452g.

38 O. J. S. Pickup, I. Khazal, E. J. Smith, A. C. Whitwood, J. M. Lynam, K. Bolaky, T. C. King, B. W. Rawe and N. Fey, *Organometallics*, 2014, **33**, 1751–1761.

39 M. R. Gyton, T. M. Hood and A. B. Chaplin, *Dalton Trans.*, 2019, **48**, 2877–2880.

40 M. J. Frisch, *et al.*, *Gaussian 09*, Gaussian Inc., Wallingford, CT, 2009 (see the full reference in ESI†).

41 D. Andrae, U. Häussermann, M. Dolg, H. Stoll and H. Preuss, *Theor. Chim. Acta*, 1990, **77**, 123–141.

42 P. C. Hariharan and J. A. Pople, *Theor. Chim. Acta*, 1973, **28**, 213–222.

43 J. P. Perdew, *Phys. Rev. B: Condens. Matter Mater. Phys.*, 1986, **33**, 8822–8824.

44 A. D. Becke, *Phys. Rev. A: At., Mol., Opt. Phys.*, 1988, **38**, 3098–3100.

45 J. Tomasi, B. Mennucci and R. Cammi, *Chem. Rev.*, 2005, **105**, 2999–3094.

46 S. Grimme, S. Ehrlich and L. Goerigk, *J. Comput. Chem.*, 2011, **32**, 1456–1465.

47 AIMALL (Version 13.02.26), TK Gristmill Software, Overland Park KS, USA, 2015.

48 A. E. Reed, J. E. Carpenter and F. Weinhold, *NBO Version 3.1*.

49 For Pathway **III**, no intermediate with bridging ^tBu or Ar' between the Rh and C_β centres was characterised. For $\text{R} = ^t\text{Bu}$, the indirect transfer of ^tBu led to the formation of the $\text{Rh}–^t\text{Bu}$ complex and for $\text{R} = \text{Ar}'$, the indirect transfer of Ar' group results in the formation of the Rh–vinylidene complex (see ESI for more details).†

50 The computed geometry features only one imaginary frequency.

51 N. A. Rajabi, PhD thesis, Heriot-Watt University, 2018.

52 N. M. Kostic and R. F. Fenske, *Organometallics*, 1982, **1**, 974–982.

53 S. M. Mansell, *Dalton Trans.*, 2017, **46**, 15157–15174.

